Electron and phonon energy spectra in a three-dimensional regimented quantum dot superlattice

Olga L. Lazarenkova* and Alexander A. Balandin†
Department of Electrical Engineering, University of California at Riverside, Riverside, California 92521
(Received 4 January 2002; revised manuscript received 12 August 2002; published 30 December 2002)

We report on theoretical investigation of the electron and phonon energy spectra in a three-dimensional regimented quantum dot superlattice. Our results are obtained by numerical solution of the Schrödinger and elasticity equations using the finite-difference method. The calculations are performed for a Ge/Si material system taking into account characteristic band-gap offsets, elastic stiffness constants, and other relevant parameters. Coupling among quantum dots in such a regimented structure results in formation of extended electron states and minibands, provided that the disorder in the system is small. Electron and phonon densities of states of these artificial *quantum dot crystals* are also calculated. We demonstrate that the acoustic-phonon dispersion in the quantum dot superlattice undergoes strong modification, which leads to emergence of quasioptical branches. These branches are much lower in energy than optical phonons in bulk semiconductors and thus may strongly affect energy relaxation processes. Other phenomena that originate from the specific electron and phonon spectra in quantum dot superlattices, such as negative differential conductivity and carrier scattering anisotropy, are also discussed.

DOI: 10.1103/PhysRevB.66.245319 PACS number(s): 73.22.−f, 63.22.+m, 73.23.−b

I. INTRODUCTION

Physical properties of individual semiconductor quantum dots (OD's) have been extensively studied both theoretically and experimentally.[1] The effects of the size, shape, strain fields, Coulomb interaction, and dielectric screening on electronic states and optical response of individual quantum dots are addressed in the literature in great detail.[1–10] In a simplified picture, transport properties of arrays of weakly coupled quantum dots (with wave functions well localized in a dot) are described in terms of hopping conduction, while optical response is defined by the energy spectrum of individual dots and inhomogeneous broadening due to the size distribution. A more interesting and potentially practically important case is when strong coupling among dots leads to formation of two- (2D) or three-dimensional (3D) extended minibands instead of localized quantum dot states. Such energy spectrum modification is expected to take place provided that (i) the quantum dots are regimented, e.g., periodicity of the quantum dots in an array is very high; (ii) the dot size is homogeneous; (iii) interdot distance and barrier height are small enough for significant electron wave-function overlap; and (iv) the dots are crystalline, with low surface defect concentration. Quantum dot structures fabricated using different techniques always have some degree of disorder, which can be described by the Anderson or Lifshitz models. At the same time, extended states and minibands can still be formed as long as the bandwidth due to wave-function overlap exceeds the total broadening, which is mostly determined by the disorder inhomogeneous broadening.

Regimented or partially regimented 2D and 3D multiple arrays of quantum dots, also termed quantum dot superlattices (QDS), have already been fabricated by a variety of techniques.[2–7,11–13] Regimentation along all three directions in a structure described in Ref. 13 brings an analogy with bulk crystals. In these artificial crystals the role of atoms is played by quantum dots. Thus, we refer to these structures as *quantum dot crystals* (QDC) or ''supra crystals.'' It is important to note that the analogy with real crystals goes further, specifically, to the carrier energy spectrum. In the discussion to follow the term quantum dot crystal is used when the intention is to emphasis that the regimentation, size, interdot distance, and quality of the dots are such that extended states are formed. As a consequence, the energy spectrum of such supra crystals is characterized by emergence of 3D minibands separated by complete stop bands or energy minigaps. The latter is not implied when the term quantum dot superlattice is used.

Formation of extended electron states and minibands have already been observed in multiple quantum dot arrays. Artemyev *et al.*[14–16] demonstrated experimentally the evolution of electron states from individual (localized) to collective (extended) states in a dense quantum dot ensemble that consisted of monodisperse small CdSe dots of average radius $R \sim 1.6-1.8$ nm arranged in a cubical or hexagonal lattice. Song *et al.*[17] investigated in-plane photocurrent in self-assembled $In_xGa_{1-x}As/GaAs$ quantum dot arrays. They reported that samples with inhomogeneous QD sizes show hopping conduction, which indicates the localization of carriers in individual dots, while the highly ordered and size-homogeneous quantum dot arrays exhibit negative differential conductance that has been attributed to carrier energy miniband formation. Yakimov *et al.*[18,19] investigated in-plane electrical conductivity of arrays of Ge quantum dots on Si with dot size $D \sim 12-19$ nm. In our preliminary study, which used an analytical solution of the Schrödinger equation for the simplified model potential, we calculated the low-field electrical conductivity in QDS (Ref. 20) and obtained good agreement with experimental curves of Refs. 18 and 19.

Apart from the fundamental scientific importance of the investigation of electron (hole) and phonon spectra in regimented quantum dot arrays, there is a significant practical interest in addressing this problem. Application of QDS as infrared photodetectors requires high values of mobility[21] in order to sweep the carriers. In the miniband transport regime one can expect much higher carrier mobility than in the hop-

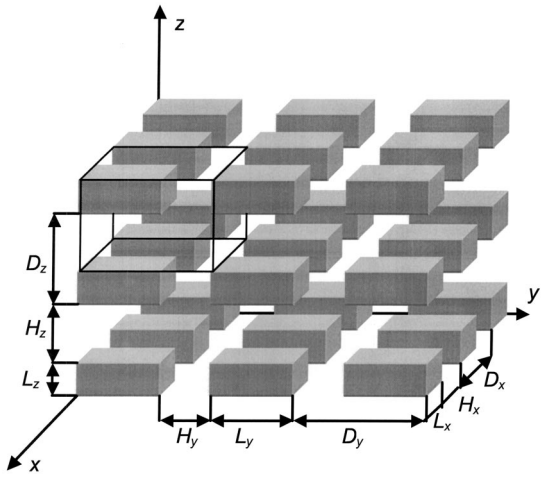

FIG. 1. Schematic structure of the orthorhombic quantum dot crystal.

ping regime.[17] Miniband conduction may also be desirable for high-temperature thermoelectric applications of quantum dot arrays.[1,22] Despite recent achievements in self-assembly of QDS and many experimental reports on electrical and optical characterizations of such structures, few theoretical papers deal with characteristics of a *regimented ensemble* of quantum dots. The reports that can be found in the literature[23–25] deal with calculation of the electronic states only under some simplifying assumptions. Most theoretical investigations are still focused on development of an accurate description of properties of a single dot.

In this paper we undertake a more general approach and investigate both *electron* and *phonon* spectra of three-dimensional regimented quantum dot superlattices using an accurate numerical solution technique. The approach proposed in this paper is a drastic improvement of our earlier semianalytical solution for the model potential.[25] Since the symmetry of the model potential is the same as in one of the considered systems, the approach described in Ref. 25 gives very good qualitative results. The semianalytical solution is useful for better understanding specific features of the electron spectrum in QDC especially below the potential barrier. On the other hand, for the subsequent calculation of the related physical properties, such as optical spectra or electrical conductivity, the absolute error of that approach is up to several dozens meV and increases significantly for the above-the-barrier states, which is unacceptable. The present calculation based on the finite-difference method (FDM) scheme allows us to accurately describe both electron and phonon spectra in 3D QDC, examine above-the-barrier states, and take disorder into consideration by extending the simulation domain above one period of the structure.

II. THEORETICAL MODEL

We consider an orthorhombic 3D-regimented quantum dot superlattice (Fig. 1) and assume that the conditions for formation of the extended carrier states are satisfied. Our goal is to investigate electron and phonon spectra of this artificial quantum dot crystal. Since we are interested in properties of a quantum dot crystal, e.g., the *regimented ensemble* of quantum dots, we limit our analysis to the simplest parallelepiped shape of the dots. The numerical solution scheme described here can be readily applied to dots of arbitrary geometry.

A. Electron spectrum

Since experimentally investigated quantum dot arrays usually have quantum dot sizes significantly larger than interatomic distances[2–7,11] we restrict our model to dots of at least a few nanometers in size. In this case we can calculate the electron spectrum of QDC in the envelope wave-function approximation applied to a potential barrier profile of choice. The one-electron Schrödinger equation for such a system is written as

$$\left[-\frac{\hbar^2}{2}\nabla_{\mathbf{r}}\frac{1}{m^*}\nabla_{\mathbf{r}}+V(\mathbf{r})\right]\varphi(\mathbf{r})=E\varphi(\mathbf{r}), \tag{1}$$

where $\hbar$ is Planck's constant, $1/m^*$ is the reciprocal effective-mass tensor, $\varphi(r)$ is the electron wave function, E is the electron energy, and the confining potential profile $V(\mathbf{r})$ corresponds to an infinite sequence of quantum dots of sizes L_x, L_y, and L_z separated by the barriers of thicknesses H_x, H_y, and H_z. The profile $V(\mathbf{r})$ is set to zero in the barrier region, while inside the quantum dot it is equal to the band offset in the conduction (or valence) band of the considered material system taken with a negative sign. The information about band structure of the host materials is reflected in the reciprocal effective-mass tensor $1/m^*$. The effect of strain was approximately taken into account by changing the value of the corresponding band offset. The confining potential $V(\mathbf{r})$ was considered to be a piecewise uniform function.

B. Phonon spectrum

Electron (hole) mobility in technologically important semiconductors such as Si or SiGe at room temperature is limited by scattering on both acoustic and optical phonons. The spectrum of optical phonons, which have high energy at the zone center, is not altered in QDC as strongly as the spectrum of acoustic phonons. There have been experimental indications that, especially at low temperatures, acoustic-phonon scattering dominates carrier relaxation in quantum dot arrays.[17] Thus, we restrict our investigation to analysis of the acoustic-phonon modes in 3D-ordered quantum dots embedded in some host material with different crystalline properties. At a long-wavelength limit, the acoustic-phonon dispersion can be described by a continuum model.

If a quantum dot structure is made of semiconductors of cubic symmetry, such as Si and Ge with a diamond lattice (O_h^7 space group) or A^3B^5 compounds such as GaAs or InAs with a zinc-blende lattice (T_d^2 space group), the number of independent elastic stiffness constants in the elasticity equation reduces to 3:

$$\rho\frac{\partial^2 u_x}{\partial t^2}=\frac{\partial}{\partial x}c_{11}\frac{\partial u_x}{\partial x}+\frac{\partial}{\partial y}c_{44}\frac{\partial u_x}{\partial y}+\frac{\partial}{\partial z}c_{44}\frac{\partial u_x}{\partial z}+\frac{\partial}{\partial x}c_{12}\frac{\partial u_y}{\partial y}$$

$$+\frac{\partial}{\partial x}c_{12}\frac{\partial u_z}{\partial z}+\frac{\partial}{\partial y}c_{44}\frac{\partial u_y}{\partial x}+\frac{\partial}{\partial z}c_{44}\frac{\partial u_z}{\partial x}. \quad (2)$$

The similar expressions for y and z components of the displacement vector $\mathbf{u}$ of a geometrical point inside the material of QDC with $(i=x,y,z)$ coordinates may be obtained by cyclic exchange of (u_x,u_y,u_z) and (x,y,z). The elasticity Eq. (2) in a nonuniform medium results from Euler-Lagrange equations for the system with a cubic crystal lattice. The solution of these equations for the quantum dot ''supra crystal'' can be expressed in a plane-wave form by analogy with regular bulk crystals,

$$\mathbf{u}(\mathbf{r},t)=\mathbf{A}(\mathbf{r})\exp[i(\mathbf{q}\cdot\mathbf{r}-\omega t)],$$

where $|\mathbf{q}|=2\pi/\lambda$ is the phonon wave vector, with phonon wavelength λ; $\mathbf{r}$ is the coordinate vector; t is time; and ω is the phonon frequency. The eigenvalues of Eq. (2) in bulk material linearly depend on the phonon wave vector, as it should be in the continuum approximation. Note that the phonon modes are of a pure compression (longitudinal) type or a pure shear (transverse) type if and only if the wave propagates along a crystallographic direction of high symmetry; otherwise it has components of each type.

The limits of the applicability of the continuum approximation can be estimated from the comparison of the calculated dispersion branches with experimental data and lattice-dynamics simulation results. Approximately, as long as acoustic-phonon dispersion remains linear the phonons can be formally treated in the continuum long-wave approximation. Based on the experimental data provided in Ref. 28, we can estimate the lowest limit for Si to be about 10 meV along the [111] crystallographic direction and about 5 meV for Ge along the same direction. It corresponds to about one-third (one-fifth) of the Brillouin zone for silicon (germanium). The latter translates to the feature size of 2–3 atomic layers in real space. Thus our approach is rather accurate for description of acoustic phonons in QDC with a feature size of several nanometers. The unit cell of the QDC of orthorhombic symmetry is analogous to the unit cell of regular bulk crystals. Using this analogy, one can solve the elasticity Eq. (2) with new quasiperiodic boundary conditions for QDC,

$$\mathbf{u}(\mathbf{r}+\mathbf{D})=\exp(i\mathbf{q}\cdot\mathbf{D})\mathbf{u}(\mathbf{r}). \quad (3)$$

Equation (3) constitutes the Bloch-Floquet theorem for an artificial quantum dot crystal, where vector $\mathbf{D}=(D_x,D_y,D_z)$ describes the new periodicity of the structure (see Fig. 1).

III. NUMERICAL APPROACH

The essence of the finite-difference method is a substitution for each differential operator in Eqs. (1) and (2), the finite-difference operator defined on a preselected grid. The common problem associated with this method is the selection of an appropriate grid to achieve the desired accuracy. In our case, due to orthorhombic symmetry of QDC and the dot shape it is convenient to use a square grid with a constant step. Since we do not consider disorder, we can limit the numerical procedure to just one period of the structure (see Fig. 2).

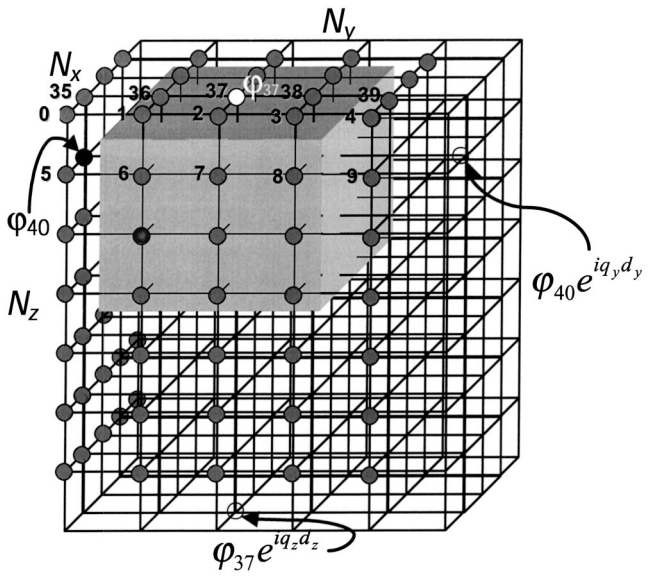

FIG. 2. Simulation domain in orthorhombic quantum dot crystals with indicated grid and boundary conditions. Eigenfunctions φ for considered partial differential equations are also shown.

Instead of n analytical partial differential equations for the whole domain we now have a set of $nN_xN_yN_z$ linear algebraic equations for the eigenfunctions φ_ξ at each ξth node of the grid. Here N_i denotes a number of nodes in the i direction. The finite-difference equations were obtained using Euler-Lagrange equations from the discretized Lagrangian of the system, which ensured the Hermiticity of the corresponding matrix constructed on bonds with material parameters determined on them. Material parameters, such as reciprocal effective mass in the Schrödinger equation and elastic stiffness constants in the elasticity equation, change abruptly at the quantum dot boundaries. The latter gives one an uncertainty in defining the difference operator if the nodal point lies on the boundary. To avoid this uncertainty we put the vertex of the quantum dot, which is the closest to the origin, to the point with coordinates $(\frac{1}{2},\frac{1}{2},\frac{1}{2})$, and further assumed that the material parameter p changes linearly from its value p_1 in one material to its value p_2 in another material. We found that the convergence is the best when the grid is chosen in such a way that the quantum dot boundaries are close to the middle of a bond.

In the FDM scheme for the Schrödinger equation we used a central difference approximation for double derivatives. The diagonal element of the QDC Hamiltonian, which corresponds to a node with coordinates (a_xj_x,a_yj_y,a_zj_z), has the following index:

$$n_{xyz}=N_xN_yj_z+N_xj_y+j_x,$$

and it is equal to

$$H_{n_{xyz}n_{xyz}} = V_{xyz} + \frac{\hbar^2}{2}\left[\frac{1}{a_x^2}\left(\frac{1}{m^*_{x+1/2,y,z}} + \frac{1}{m^*_{x-1/2,y,z}}\right) + \frac{1}{a_y^2}\left(\frac{1}{m^*_{x,y+1/2,z}} + \frac{1}{m^*_{x,y-1/2,z}}\right) + \frac{1}{a_z^2}\left(\frac{1}{m^*_{x,y,z+1/2}} + \frac{1}{m^*_{x,y,z-1/2}}\right)\right].$$

Note that values of V and m^* vary as the functions of the node coordinates. The nodes with coordinates $[a_x(j_x+1), a_y j_y a_z j_z]$, $[a_x j_x, a_y(j_y+1), a_z j_z]$, and $[a_x j_x, a_y j_y, a_z(j_z+1)]$ form the bonds along x, y, and z directions, respectively. The corresponding elements in the Hamiltonian are

$$H_{n_{xyz}n_{(x+1)yz}} = -\frac{r_x}{m^*_{x+1/2,y,z}a_x^2}\hbar^2/2,$$

$$H_{n_{(x+1)yz}n_{xyz}} = -\frac{\overline{r_x}}{m^*_{x+1/2,y,z}a_x^2}\hbar^2/2, \quad (4)$$

$$H_{n_{xyz}n_{x(y+1)z}} = -\frac{r_y}{m^*_{x,y+1/2,z}a_y^2}\hbar^2/2,$$

$$H_{n_{x(y+1)z}n_{xyz}} = -\frac{\overline{r_y}}{m^*_{x,y+1/2,z}a_y^2}\hbar^2/2, \quad (5)$$

$$H_{n_{xyz}n_{(z+1)yz}} = -\frac{r_z}{m^*_{x,y,z+1/2}a_z^2}\hbar^2/2,$$

$$H_{n_{xy(z+1)}n_{xyz}} = -\frac{\overline{r_z}}{m^*_{x,y,z+1/2}a_z^2}\hbar^2/2. \quad (6)$$

Here the phase shift r_ξ is equal to unity everywhere except for the points with $j_\xi = N_\xi$, where the phase shift is given by the expression

$$r_\xi = \exp(iq_\xi d_\xi).$$

In the above Eqs. (4)–(6) $\overline{r_\xi}$ is the complex conjugate of r_ξ. Due to its locality the finite-difference version of the Schrödinger equation has only seven nonzero elements per row in the QDC electron (hole) Hamiltonian of $(N_xN_yN_z) \times (N_xN_yN_z)$ size.

The FDM scheme for elasticity Eq. (2) is more complicated than for Schrödinger Eq. (1) since it contains mixed derivatives. The corresponding matrix has 35 nonzero elements in each $3(N_xN_yN_z)$ row.

To find the eigenvalues of the matrices generated for electron states and phonon modes we used the ARPACK software package.[29] It uses the implicitly restarted Arnoldi method[30] designed to solve large-scale eigenvalue problems and allows one to diagonalize the sparse matrices such as those described in this section.

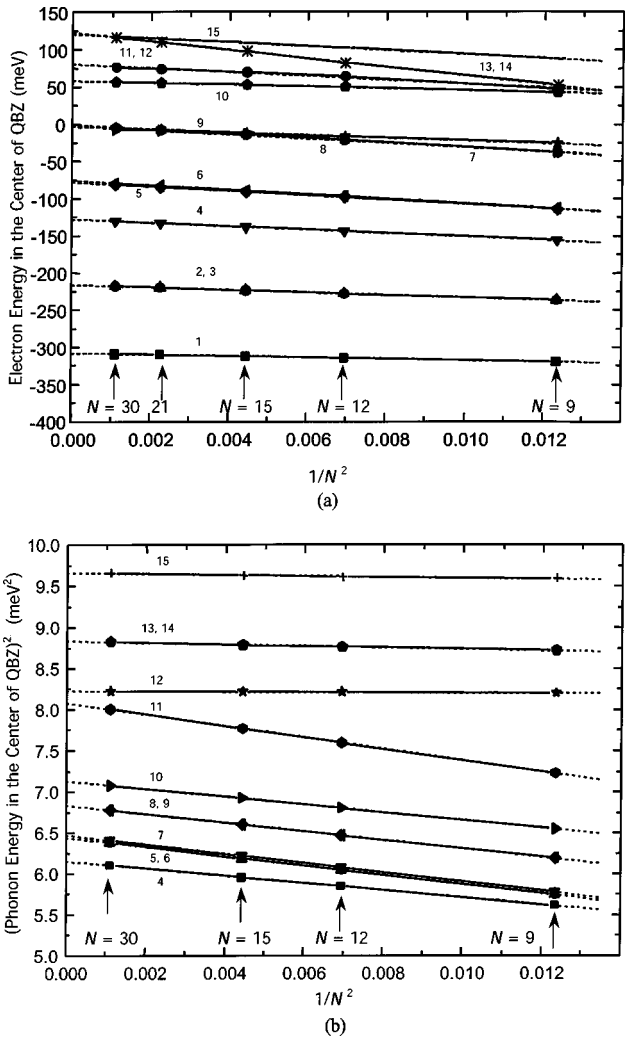

FIG. 3. Dependence of the eigenvalues of Schrödinger (a) and elasticity (b) equations at the center of the quasi-Brillouin zone of Ge/Si QDC with the following parameters: $L_x = L_y = 5$, $L_z = 2.5$, $H_x = H_y = 2.5$, and $H_z = 1.25$ nm as a function of the inverse squared number of nodes in every direction. The dashed lines are linear extrapolations of the dependencies to zero. The zero point corresponds to the infinite number of nodes and thus the extrapolated eigenvalues are close to the "true" ones.

IV. RESULTS AND DISCUSSION

As an example of a material system we consider Ge quantum dots grown on Si by molecular-beam epitaxy (MBE). Although state-of-the-art Ge/Si QDS are characterized only by partial regimentation,[4,5] continuous progress in MBE self-assembly most likely will lead to synthesis of 3D-regimented quantum dot superlattices similar to those reported in Refs. 12 and 13. We have carried out numerical simulations for QDC with the following parameters: $L_x = L_y = 5.0$, $L_z = 2.5$, $H_x = H_y = 2.5$, and $H_z = 1.25$ nm; $m^B_{hh} = 0.49m_0$, $m^W_{hh} = 0.28m_0$, and $V_{hh} = 0.450$ eV. For simplicity we restrict our analysis to heavy holes in Ge/Si QDC. This is done for two reasons. First, most of the band-gap discontinuity between Si and Ge goes to the valence band. Secondly, we can use the single-valley effective mass approximation since a single

potential energy maximum in the valence band is located in Γ point.

A. Accuracy of the FDM scheme

First, we verify the accuracy of the results obtained using the outlined approach. The most important question when dealing with numerical methods is dependence of the results on the grid step, i.e., convergence of the developed FDM scheme. Three-dimensional periodicity of QDC structure dramatically reduces the number of nodes necessary for a good convergence of the finite-difference scheme compared to a single quantum dot task.

Figures 3(a) and 3(b) show the dependence of the eigenvalues of Schrödinger [Fig. 3(a)] and elasticity [Fig. 3(b)] equations at the center of the quasi-Brillouin zone (QBZ) as a function of the inverse squared number of nodes N in every direction. The zero point corresponds to the infinite number of nodes and thus the extrapolated eigenvalues are close to the ''true'' ones. The relative error δ for $N=15$ (i.e., only five nodes in barriers and ten inside dots) varies in the range 0.31%–4.01% for elasticity Eq. (2) eigenvalues and 0.32%–1.97% for phonon energies, correspondingly. The electron energy relative error for $N=15$ is 1.04%–4.45%. If the number of nodes increases to 30, the error reduces to 0.33%–1.12% for electron and 0.00%–0.93% for phonon energies. Thus it is enough to have as few as five to ten nodes inside a single quantum dot and in the spacer to achieve accuracy better than 5% for the energy. Such good convergence makes it possible in the future to take disorder into consideration by expanding the simulation subdomain to several periods of QDC. Nevertheless we choose to use $N=30$ in our calculations for the system without disorder.

B. Electron spectrum in QDC

Solid lines in Figs. 4(a) and 4(b) show the heavy-hole dispersion of Ge/Si QDC calculated using the FDM outlined in Sec. III. The energy is given with respect to the position of the potential barrier. Double brackets for the wave-vector notation are introduced to distinguish direction in quantum dot supra crystals from crystallographic directions. For comparison, we also present the heavy-hole dispersion (dashed lines) in Ge/Si QDC with the same material parameters and dot size but calculated for the model potential using our semianalytical approach.[25] This model potential of the type $V(x,y,z)=V(x)+V(y)+V(z)$, which approximates the ''conventional'' uniform-height potential barrier of QDC, allows for wave-function coordinate separation and analytical solution.[19,25,26] The three-digit numbers $n_x n_y n_z$ near the curves indicate the symmetry of the corresponding wave functions. The number of zeros in the ξ direction is equal to $(n_\xi-1)$. One can see that the analytical solution agrees well with the FDM solution for below-the-barrier states. Arrows indicate the energy difference between corresponding states. Since the relative error for 30 nodes in every direction is very small ($\leqslant 1\%$), we can say that some discrepancy of these solutions is mostly due to the difference in the confining potentials used in Ref. 25, where we chose to allow for wave-function separation. The relative error of the electron

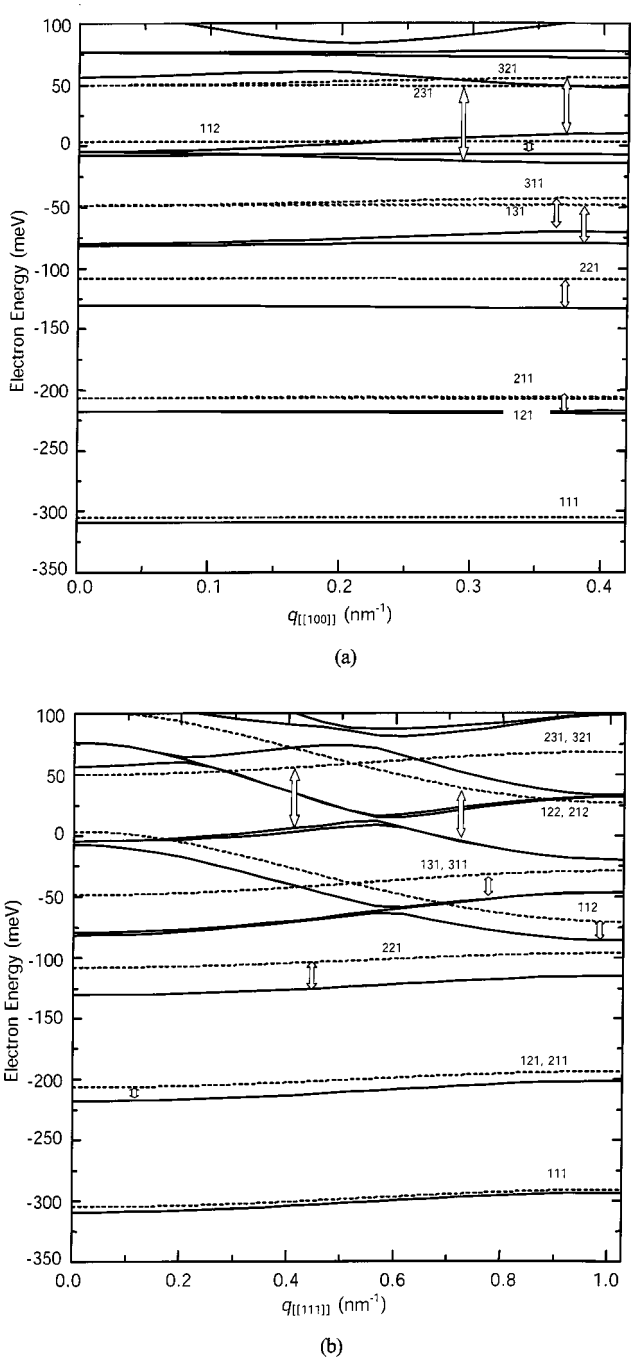

FIG. 4. Heavy-hole dispersion in Ge/Si QDC with the following parameters: $L_x=L_y=5$, $L_z=2.5$, $H_x=H_y=2.5$, and $H_z=1.25$ nm along the [[100]] quasicrystallographic direction (a) and along the [[111]] quasicrystallographic direction (b). Solid lines show the dispersion found using the finite-difference method. Dashed lines show the dispersion found for a model potential that allows for wave-function separation in the Schrödinger equation. Heavy-hole minibands on the plot are indicated by the three quantum numbers. Arrows show the correspondence of these two solutions. The energy in units of eV is counted from the position of the potential barrier. Note that below-the-barrier states obtained by different methods are close.

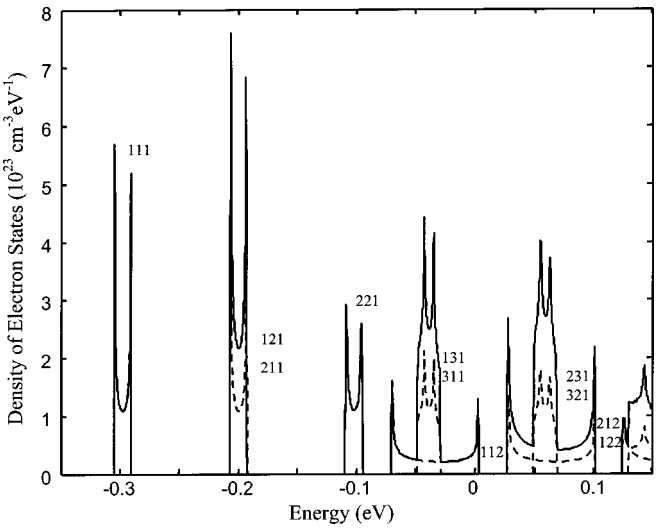

FIG. 5. Density of heavy-hole states calculated separately for each miniband in the tetragonal Ge/Si QDC with the parameters $L_x=L_y=5$, $L_z=2.5$, $H_x=H_y=2.5$, and $H_z=1.25$ nm shown with the dashed line. Their sum corresponding to the total density of states is shown with the solid line.

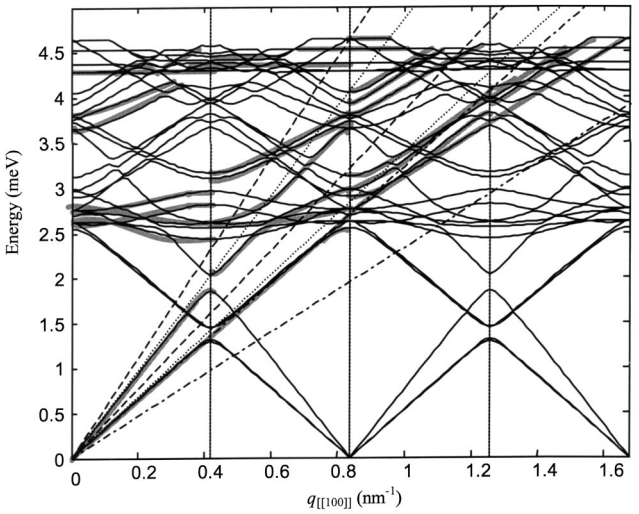

FIG. 6. Phonon dispersion in Ge/Si 3D regimented quantum dot superlattice (solid lines) plotted for a structure with the following parameters: $L_x=L_y=5.0$, $L_z=2.5$, $H_x=H_y=2.5$, and $H_z=1.25$ nm. The dispersion is shown along the [[100]] quasicrystallographic direction. Acoustic-phonon dispersion relations in bulk Si and Ge are indicated with dashed and dot-dashed lines, correspondingly. Dotted lines show the acoustic-phonon dispersion estimated from the volume fractions of Si and Ge in given QDC.

energy found by this method in the center of the QBZ is 1.32%–11.91% and the corresponding deviation in energy varies from 3.1 to 53.2 meV. One can also notice that the FDM solution allows one to lift the degeneracy of some dispersion branches away from the points of high symmetry. On the other hand, the accurate FDM solution presented here can be used as a validation procedure for simpler and faster analytical solution with separable model potential, which may be more practical for the below-the-barrier states.

Similar to bulk crystals, the energy dispersion in QDC has the full symmetry of the reciprocal lattice. In this artificial crystal some of the energy bands are degenerate in the center of the QBZ. Moving away from the point of high symmetry in the center of the QBZ to a point of lower symmetry splits the energy branches [see, for example, the second from the bottom dispersion branch in the [[100]] quasicrystallographic direction in Fig. 4(a)].

Figure 5 illustrates the electron density of states (DOS) found using the simplified analytical solution and conventional definition

$$G(E)=\frac{2}{dE}\int d^3\mathbf{k}.$$

Here the integral is taken over the volume in **k** space bounded by a surface of constant energy *E*. Coupling among regimented quantum dots leads to a drastic change in the electron DOS as compared to single dots or quantum well superlattices. The double peaks seen in Fig. 5 correspond to the same electron miniband. The stronger the interdot interaction, the larger the energy spacing between the peaks. For a given structure the energy spacing is several dozens of meV. In quantum well superlattices the electron DOS has an arccosinelike form superimposed over a characteristic ''staircase'' due to a 2D electron continuum in planes perpendicular to the growth direction. This is not the case for a quantum dot crystal. Although for the lowest miniband the DOS in the artificial crystal has an arccosinelike edge, it drops to zero at some higher energy since there is not 2D continuum, and it becomes much more complicated for higher-energy minibands (Fig. 5). On the other hand, the shape of the DOS in QDC is evidently different from a delta-function-like DOS of single quantum dots or a *random* array of noninteracted quantum dots. Despite the analogy in shape to the DOS of regular bulk crystals, the energy scale for DOS peaks in quantum dot crystals is a thousand times smaller.

C. Phonon spectrum in QDC

Figure 6 presents the phonon dispersion in the [[100]] quasicrystallographic direction calculated using the FDM. This quasicrystallographic direction in QDC is parallel to the [100] crystallographic direction in the host material, assuming that the QDC structure is grown on the (001)-oriented substrate. The phonon spectrum in Fig. 6 is presented in the extended Brillouin-zone scheme to emphasize the existence of two different types of phonon modes in QDC that emanate from bulk acoustic modes. These modes are quasiacoustic $[\omega(\mathbf{q}=0)=0]$ and quasioptical $[\omega(q=0)\neq 0]$.

Quasiacoustic modes are nothing else but folded acoustic branches of the host material. The multiple reflection of phonons from periodic interfaces leads to a minigap formation at the Brillouin-zone boundary. The degeneracy due to intersection of different branches is lifted everywhere except for the points of high symmetry. The same figure shows the acoustic-phonon dispersion in bulk Si (dashed lines) and bulk Ge (dot-dashed lines) along the [100] crystallographic direction. The longitudinal and transverse sound velocities are assumed to be $\nu_L=8433.2$ and $\nu_T=5844.6$ m/s for Si,

and $\nu_L = 4913.8$ and $\nu_T = 3542.4$ m/s for Ge,[28] respectively. The value of the group velocity for the quasiacoustic phonons in QDC lies between Si and Ge sound velocities and it is not defined by the volume fractions of two constituent materials (see the dotted lines in Fig. 6). Even in solid alloys where atoms of two materials are randomly distributed elastic properties change almost linearly only in ''one-mode behaved'' systems such as $Na_{1-x}K_xCl$.[27] The composition dependence of phonon energy in the Si_xGe_{1-x} alloy is far from linear.[28] In systems with a spatial regimentation like in QDC the deviation from linear dependence should increase.

The quasiacoustic dispersion branches deviate downwards from the linear dependence at higher phonon energy. The transverse mode, which is doubly degenerate at the zone center, splits at the zone boundary. If the wave propagates along the [[100]] quasicrystallographic direction in QDC with tetragonal symmetry ($d_x = d_y \neq d_z$), two shear modes [[010]] and [[001]] are different. If $d_y > d_z$ the [[010]] mode bends more strongly than the [[001]] mode. However, if the phonon wavelength λ is large compared to the QDC period $|\mathbf{d}|$, e.g., $\lambda = 2\pi/|\mathbf{q}| \gg |\mathbf{d}|$, acoustic wave properties are determined by the averaged medium parameters (effective-medium approximation) and the fine structure of the medium does not strongly affect the wave propagation. Indeed, this is clearly seen in the extended zone presentation when the phonon wave vector approaches the third Brillouin zone, which corresponds to the period of the quantum dot superlattice $d_x = 7.5$ nm along this direction. At this value of the wave vector, the slope of the quasiacoustic modes that defined the group velocity increases.

Quasioptical modes correspond to ''nearly standing'' waves. One can view them as created by periodic scatters such as quantum dot interfaces. These modes can be induced inside quantum dots or in the space between them. A ''true'' standing wave would have a completely flat dispersion relation, which reflects the fact that this wave does not propagate through the crystal. In contrast, the dispersion branches of quasioptical modes can have a minimum. The latter means that these modes propagate slowly going back and forth. We refer to these modes as quasioptical since they have a nonzero energy in the center of the Brillouin zone, e.g., a cutoff frequency. At the same time one should emphasize that these modes are also emanating from acoustic bulk phonon modes. The regular optical-phonon modes have much higher energy. In Ge/Si QDC of the considered geometry the lowest quasioptical branch has the energy of about 2.6 meV at the zone center. In bulk Si the longitudinal-optical (LO) and transverse-optical (TO) phonon energies are $\hbar\omega^{\Gamma}_{\mathrm{LO}} = \hbar\omega^{\Gamma}_{\mathrm{TO}} = 64.3$ meV. In bulk Ge they are $\hbar\omega^{\Gamma}_{\mathrm{LO}} = \hbar\omega^{\Gamma}_{\mathrm{TO}} = 37.2$ meV.[28] It is obvious that emergence of many quasioptical phonon branches in QDC that have low characteristic energy may dramatically modify carrier energy relaxation processes in such structures. This is somewhat analogous to the change that electron-phonon interaction undergoes in semiconductor quantum wires.[31–33]

D. Tuning transport properties of quantum dot *supra* crystals

Unlike ''real'' crystals where atoms, lattice geometry, and interatomic distances are fixed entities, quantum dot supra

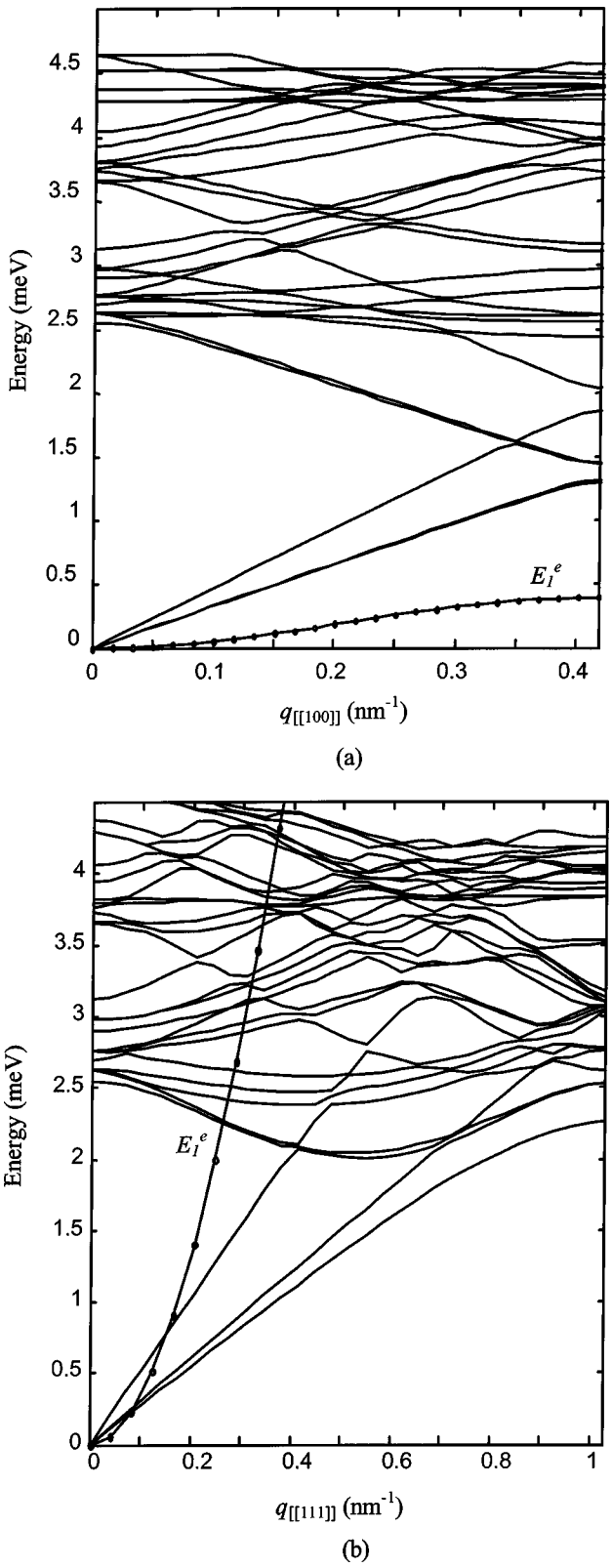

FIG. 7. Phonon dispersion (solid lines) and the first heavy-hole miniband (solid line with dots) shown along [[100]] (a). [[111]] (b) quasicrystallographic directions in Ge/Si QDC with the following parameters: $L_x = L_y = 5.0$, $L_z = 2.5$, $H_x = H_y = 2.5$, and $H_z = 1.25$ nm. For convenience, the heavy-hole energy is counted from the miniband minimum.

crystals represent ensembles of designer atoms with potential for tuning their transport and optical properties. As an example, we analyze here a possibility of achieving suppression or anisotropy of some types of electron-phonon scattering in QDC. Suppression of electron-phonon scattering could be beneficial for a variety of reasons, from improved prospects for observation of Bloch oscillations[23] to applications of Ge/Si QDC in photodetectors and thermoelectric devices. The important parameters of the carrier band structure that defines electron-phonon scattering are the (first) miniband half width Δ_1 and the energy gap between the first two minibands E_2-E_1.

Let us consider single-phonon-assisted processes, which are usually the most important ones. We compare heavy-hole and phonon-dispersion branches along [[100]] and [[111]] quasicrystallographic directions [see Figs. 7(a) and 7(b)]. The first heavy-hole branches are shown with solid lines (marked with circles). A hole (or an electron) can scatter from its initial state $E(\mathbf{k}_i)$ to the final state $E(\mathbf{k}_f)$ with phonon $\hbar\Omega(\mathbf{q})$ assistance if and only if both energy-conservation $E(\mathbf{k}_f)-E(\mathbf{k}_i)=\hbar\Omega(\mathbf{q})$ and momentum-conservation $\mathbf{k}_f-\mathbf{k}_i=\mathbf{q}$ laws are satisfied. Assuming a linear acoustic-phonon dispersion for small wave vectors, e.g., $\hbar\Omega(\mathbf{q})=\hbar\mathbf{v}_g\mathbf{q}$, one can find from the above equations the condition for the allowed acoustic-phonon-assisted transitions:

$$\frac{E(\mathbf{k}_f)-E(\mathbf{k}_i)}{\hbar|\mathbf{k}_f-\mathbf{k}_i|}=\nu_g. \tag{7}$$

Equation (7) can be graphically interpreted as a horde to the hole dispersion with the slope equal to the acoustic-phonon group velocity. In tetragonal ($d_x=d_y>d_z$) QDC the heavy-hole and phonon dispersion along [[100]] [see Fig. 7(a)] and [[010]] directions generally have the smallest value of the slope, while [[111]] [see Fig. 7(b)] is the direction of the steepest branches. As one can see in Fig. 7(a) for given parameters of QDC there are no phonons available that can scatter holes within the same (first) miniband. Roughly, this is because the hole miniband is very flat. Along the [[111]] quasi-crystallographic direction [see Fig. 7(b)] the slope of the first hole miniband is much larger than the phonon group velocity of any branch. It results in scattering suppression in approximately 80% of the Brillouin zone except for the small areas near the center and the Brillouin-zone boundary. Thus, the hole-single-phonon scattering in QDC displays spatial anisotropy.

Interminiband transitions with assistance of one phonon are forbidden for the considered structure. The minigap between the first two minibands shown in Fig. 4, $E_2-E_1 \sim 80-100$ meV, is larger than the optical-phonon energy even in the bulk host material ($\hbar\omega^{\Gamma}_{\mathrm{LO}}=\hbar\omega^{\Gamma}_{\mathrm{TO}}=64.3$ meV for Si and $\hbar\omega^{\Gamma}_{\mathrm{LO}}=\hbar\omega^{\Gamma}_{\mathrm{TO}}=37.2$ meV for Ge[28]). At the same time, multiphonon scattering in QDC may play a significant role in energy relaxation processes due to the presence of many quasioptical-phonon branches (see Figs. 6 and 7). At room temperature, these low-energy branches should have a high population density in accordance with Bose-Einstein statistics.

Analyzing obtained numerical results (see Fig. 4) we are able to make the following important observation. The existence of 3D minibands in quantum dot superlattices may result in nonlinear dependence of electrical conductivity on the applied bias. The latter follows from the various possibilities for position of the quasi-Fermi level (QFL) with respect to miniband edges. When the QFL is below the first miniband or lies in a gap between minibands, QDC manifest quasiinsulator or quasisemiconductor properties depending on the temperature. When the QFL is inside a miniband, QDC exhibit quasimetallic properties. This changing behavior may lead to quasiphase transitions and *negative differential conductivity* of regimented quantum dot structures. The negative differential conductance in self-assembled In_xGa_{1-x}-As/GaAs quantum dot arrays has recently been measured at a temperature of 4.5 K.[17]

V. CONCLUSIONS

We obtained the electron (hole) and phonon energy spectra in a three-dimensional regimented quantum dot superlattice by solving the Schrödinger equation in the envelope wave-function approximation and elasticity equation in the continuum approximation. Both equations have been solved numerically using the finite-difference method. Electron (hole) and phonon densities of states, required for modeling of transport and optical properties of quantum dot superlattices, were also calculated. Three-dimensional regimentation of quantum dots in such superlattices brings a number of interesting analogies with bulk semiconductor crystals. Coupling among quantum dots in such a regimented structure, e.g., quantum dot crystal, results in formation of extended electron states and minibands provided that the disorder in the system is small. We demonstrate that the acoustic-phonon dispersion in the quantum dot superlattice undergoes strong tunable modification, which leads to emergence of quasioptical branches. These branches are much lower in energy than ''true'' optical phonons in bulk semiconductors and thus may strongly affect energy relaxation processes. We also discussed some important phenomena that originate from the specific electron and phonon spectra in quantum dot superlattices, such as negative differential conduction, carrier-phonon scattering anisotropy, and suppression.

Note Added in Proof. We learned about a recent theoretical study[34] that suggests that minibands in quantum dot superlattices are rather robust against morphological or configurational disorder, which adds validity to the assumptions made in this work.

ACKNOWLEDGMENTS

This material is based upon work supported in part by the National Science Foundation under CAREER Award No. 0093959 to A.A.B., and AFOSR STTR Contract No. F49620. O.L. is indebted to Professor L.P. Pryadko (UCR) for his help with numerical solution.

*On leave from the Microelectronics Department, St. Petersburg State Electrotechnical University ''LETI,'' St. Petersburg, Russia.

†Corresponding author. Electronic address: alexb@ee.ucr.edu

[1] For a review, see, for example, K. L. Wang and A. Balandin, Quantum Dots: Properties and Applications, in *Optics of Nanostructured Materials*, edited by V. Markel and T. George (Wiley, New York, 2000), p. 515.

[2] N. N. Ledentsov, V. M. Ustinov, V. A. Shchukin, P. S. Kop'ev, Zh. I. Alferov, and D. Bimberg, Semiconductors **32**, 343 (1998).

[3] V. Ya. Aleshkin, N. A. Bekin, N. G. Kalugin, Z. F. Krasilnik, A. V. Novikov, V. V. Postnikov, and H. Seyringer, Pis'ma Zh. Eksp. Teor. Fiz. **67**, 46 (1998) [JETP Lett. **67**, 48 (1998)].

[4] J. L. Liu, W. G. Wu, A. Balandin, G. L. Jin, and K. L. Wang, Appl. Phys. Lett. **74**, 185 (1999).

[5] J. L. Liu, W. G. Wu, A. Balandin, G. Jin, Y. H. Luo, S. G. Thomas, Y. Lu, and K. L. Wang, Appl. Phys. Lett. **75**, 1745 (1999).

[6] P. C. Sharma, K. W. Alt, D. Y. Yeh, D. Wang, and K. L. Wang, J. Electron. Mater. **28**, 432 (1999).

[7] A. Balandin, S. Bandyopadhyay, P. G. Snyder, S. Stefanovich, G. Banerjee, and A. E. Miller, Phys. Low-Dimens. Semicond. Struct. **11/12**, 155 (1997).

[8] T. Takagahara, Phys. Rev. B **47**, 4569 (1993).

[9] E. P. Pokatilov, V. A. Fonoberov, V. M. Fomin, and J. T. Devreese, Phys. Rev. B **64**, 245328 (2001).

[10] V. M. Fomin, V. N. Gladilin, J. T. Devreese, E. P. Pokatilov, S. N. Balaban, and S. N. Klimin, Phys. Rev. B **57**, 2415 (1998).

[11] A. Balandin, K. L. Wang, N. Kouklin, and S. Bandyopadhyay, Appl. Phys. Lett. **76**, 137 (2000).

[12] S. Facsko, T. Dekorsy, C. Koerdt, C. Trappe, H. Kurz, A. Vogt, and H. L. Hartnagel, Science **285**, 1551 (1999).

[13] G. Springholz, M. Pinczolits, P. Mayer, V. Holy, G. Bauer, H. H. Kang, and L. Salamanca-Riba, Phys. Rev. Lett. **84**, 4669 (2000).

[14] M. V. Artemyev, A. I. Bibik, L. I. Gurinovich, S. V. Gaponenko, and U. Woggon, Phys. Rev. B **60**, 1504 (1999).

[15] M. V. Artemyev, U. Woggon, H. Jaschinski, L. I. Gurinovich, and S. V. Gaponenko, J. Phys. Chem. B **104**, 11 617 (2000).

[16] M. V. Artemyev, A. I. Bibik, L. I. Gurinovich, S. V. Gaponenko, H. Jaschinski, and U. Woggon, Phys. Status Solidi B **224**, 393 (2001).

[17] H. Z. Song, K. Akahane, S. Lan, H. Z. Xu, Y. Okada, and M. Kawabe, Phys. Rev. B **64**, 085303 (2001).

[18] A. I. Yakimov, V. A. Markov, A. V. Dvurechenskii, and O. P. Pchelyakov, Pis'ma Zh. Eksp. Teor. Fiz. **63**, 423 (1996) [JETP Lett. **63**, 444 (1996)].

[19] A. I. Yakimov, V. A. Markov, A. V. Dvurechenskii, and O. P. Pchelyakov, J. Phys.: Condens. Matter **6**, 2573 (1994).

[20] O. L. Lazarenkova and A. A. Balandin, in *Proceedings of the Electrochemical Society*, edited by M. Cahay, J. P. Leburton, D. J. Lockwood, S. Bandiopadhyay, and J. S. Harris (Electrochemical Society, Pennington, NJ, 2001), Vol. 19, p. 238.

[21] E. Towe and D. Pan, IEEE J. Quantum Electron. **6**, 408 (2000).

[22] T. C. Harman, P. J. Taylor, T. L. Spears, and M. P. Walsh, J. Electron. Mater. **29**, L1 (2000).

[23] I. A. Dmitriev and R. A. Suris, Semiconductors **35**, 212 (2001).

[24] C. Goffaux, V. Lousse, and J. P. Vigneron, Phys. Rev. B **62**, 7133 (2000).

[25] O. L. Lazarenkova and A. A. Balandin, J. Appl. Phys. **89**, 5509 (2001).

[26] O. L. Lazarenkova and A. A. Balandin, in Proc. Mater. Res. Soc. **677**, AA4.4 (2001).

[27] K. B. Böer, *Survey of Semiconductor Physics* (Van Nostrand Reinhold, New York, 1990).

[28] *Physics of Group IV Elements and III-V Compounds*, edited by O. Madelung, M. Schulz, and H. Weiss, Landolt-Börnstein, New Series, Group III, Vol. 17, Pt. (a) (Springer-Verlag, Berlin, 1982).

[29] R. B. Lehoucq, D. C. Sorensen, and P. Vu. *ARPACK: An Implementation of the Implicity Re-started Arnoldi Iteration That Computes Some of the Eigenvalues and Eigenvectors of a Large Sparce Matrix* (Rice University, 1995). R. B. Lehoucq, D. C. Sorensen, and C. Yang, *ARPACK User's Guide: Solution of Large-Scale Eigenvalue Problems with Implicit Restarted Arnoldi Methods* (SIAM, Philadelphia, 1998). Standard ARnoldi PACKage (ARPACK) software package is available free of charge at http://www.caam.rice.edu/software/ARPACK/

[30] *Large Scale Matrix Problems*, edited by Å. Björk, R. J. Plemmons, and H. Schneider (Elsever, New York, 1981).

[31] A. Svizhenko, A. Balandin, S. Bandyopadhyay, and M. A. Stroscio, Phys. Rev. B **57**, 4687 (1998).

[32] A. Svizhenko, S. Bandyopadhyay, and M. A. Stroscio, J. Phys.: Condens. Matter **10**, 6091 (1998).

[33] J. Zou and A. Balandin, J. Appl. Phys. **89**, 2932 (2001).

[34] I. Gomez, F. Dominguez-Adame, E. Diez, and P. Orellana, J. Appl. Phys. **92**, 4486 (2002).